Polarization of high-order harmonics

Philippe Antoine,[1,2] Bertrand Carré,[1] Anne L'Huillier,[1,3] and Maciej Lewenstein[1]
[1]*Commissariat à l'Energie Atomique, DSM/DRECAM/SPAM, Centre d'Etudes de Saclay, 91191 Gif-sur-Yvette, France*
[2]*Laboratoire de Physique Atomique et Moléculaire, Université Catholique du Louvain, Chemin du Cyclotron, 2 B-1348 Louvain-la-Neuve, Belgium*
[3]*Department of Physics, Lund Institute of Technology, S-221 00 Lund, Sweden*
(Received 16 April 1996; revised manuscript received 25 October 1996)

We report measurements and calculations of the polarization state of high-order harmonics generated by a 790-nm Ti:sapphire laser. The problem of completely characterizing the polarization state of a partially polarized radiation in the XUV range is discussed in detail. The comparison between several gases, xenon, argon and neon, and different orders, from the 17th to the 33rd, shows that the rotation angle and ellipticity strongly depends on the position of the harmonic in the spectrum, and in particular, whether it is in the cutoff or in the plateau. In the plateau, the rotation angle is quite large, and the ellipticity follows that of the fundamental, remaining, however, smaller. The radiation is only partially polarized. In contrast, in the cutoff, both rotation angle and ellipticity remain small, independently of the laser ellipticity. Our experimental results compare well with theoretical predictions including the single-atom response and propagation effects. [S1050-2947(97)07902-X]

PACS number(s): 32.80.Rm, 42.65.Ky

I. INTRODUCTION

High-order harmonic generation provides an efficient source of radiation in the extreme ultraviolet (XUV) region. It is also a probe of the behavior of an atom in an intense laser field. The recognizable features of harmonic spectra, in particular the extended plateau followed by the sharp cutoff, are predicted by many theoretical models. More severe tests are required to differentiate among them and hence to improve the understanding of the process. Polarization measurements provide such a test.

The interpretation of high-order harmonic generation processes is usually given by the two-step quasiclassical description [1,2]. In this model, the electron tunnels out through the potential barrier lowered by the laser field. Its subsequent motion can be treated classically and consists of free oscillations driven by the electric field. If the electron returns close to the nucleus, it may recombine and emit a harmonic photon. The limit of the plateau is therefore determined by the maximum kinetic energy gained by the electron. According to this model, in order to control harmonic generation process, one has to control the motion of the free electron. Shaping appropriately the electron trajectories allows for various future interesting perspectives.

A simple way to alter the trajectory of the oscillating electron is to use elliptical polarization instead of linear polarization. With a linear polarization, in the semiclassical picture, the electron passes periodically through the core where harmonics are radiated. With elliptical polarization, such trajectories do not exist. In fact, harmonic generation is only possible due to the extent of the wave packet and to quantum diffusion. Therefore, the harmonic generation efficiency decreases very rapidly when the ellipticity of the light is increased. This behavior has been experimentally observed by several groups [3–6]. The strong dependence of the harmonic conversion efficiency with the laser degree of ellipticity has been used to control the angular emission of the harmonics, by modulating the laser ellipticity in the focal region [7]. Similarly, it has been suggested that by modulating in time the laser degree of ellipticity, extremely short (subfemtosecond) pulses of light could be produced [8]. Both ideas are based on the fact that harmonics are produced almost only where or when the polarization of the laser is linear.

The harmonic radiation generated by an elliptically polarized driving field is also elliptically polarized. In the perturbative regime, its polarization follows the polarization of the driving field. This is not true in general at high laser intensity, in a nonperturbative regime. Weihe *et al.* observed that the polarization ellipse of low-order harmonics was rotated with respect to the ellipse of the driving field [9]. This effect was theoretically demonstrated for higher-order harmonics [10,11]. We also predicted that the ellipticity of high-order harmonics was, in general, smaller than that of the driving field. The polarization state of the harmonic radiation generated by an elliptically polarized driving field is much more sensitive to the dynamics of the process than, for example, the overall conversion efficiency, thus providing a critical test for theoretical models.

In this paper, we address the problem of measuring the polarization of the harmonics. We extend the results of Weihe *et al.* [9] on the rotation of the polarization ellipse to much higher harmonic orders. We also study how the degree of ellipticity of the generated radiation depends on the laser ellipticity. A major point that we want to emphasize is that our experimental analysis accounts for the fact that the polarization of the harmonic field is *not uniform* in space, i.e., in the plane transverse to the propagation direction, and in time, over the duration of the pulse. As shown in our theoretical study [10], this nonuniformity comes from the fact that the Fourier components of the single-atom dipole moment, sources for the harmonic emission, rapidly vary, both in phase and amplitude, with the laser intensity. The experimental measurements concern of course the total field, i.e., integrated in time, over the pulse width and in space, in the

transverse direction. Because of the nonuniformity, the integrated field is only *partially polarized*. The rotation angle and ellipticity describe the state of polarization of the polarized part of the radiation [15]. The complete determination of the polarization state of a partially polarized electromagnetic field requires much more effort than for a completely polarized field, in particular for radiation in the XUV range. Our measurements allowed us to determine the rotation angle of the harmonic radiation and to give an upper value to the degree of ellipticity. We performed extensive numerical simulations reproducing the experimental procedure for the (partial) determination of the polarization of the harmonic field.

While electron rescattering by the atomic potential is originally not included in the model, the comparison with experiment is improved by taking account of rescattering in an effective way [13]. To that condition, the numerical results reproduce the rotation angle very well. For the upper value of the ellipticity, its variations with the harmonic order are qualitatively reproduced, but in general, the calculated value is found to be lower than the measured one. The overall reasonable agreement allows one nevertheless to estimate the calculated ellipticity and the degree of polarization for the partially polarized light.

The paper is organized as follows. In Sec. II, we recall briefly the theoretical model used in the simulations [10]. We describe in particular the different measurements (or calculations) required to determine the polarization of the harmonic field. Section III gives a description of the experimental setup and procedure. Finally, in Sec. IV, we compare experimental results with theoretical predictions.

II. THEORY

We first summarize our theoretical approach, then how to determine the polarization of the harmonics.

A. Theoretical approach

In the single-atom response, we consider an atom in a single-electron approximation under the influence of a laser field $\mathcal{E}(t)$ of arbitrary polarization. Our model is a version of the so-called strong-field approximation [12]. We describe the time-dependent system in the basis reduced to the ground state and the free continuum states, i.e., the free waves eigenstates of the momentum $\vec{p}$ unperturbed by the atomic potential (in that respect, Coulomb scattering of the electron is not included in the model).

Our approach is valid in a tunneling regime, i.e., a low-frequency, high intensity regime. This model, which recovers the two-step interpretation, includes rigorously quantum tunneling, quantum diffusion, and interference. The time-dependent dipole moment is expressed as [10]

$$\vec{x}(t)=i\int_0^t dt' \int d^3\vec{p}\,\vec{d}^{\,*}(\vec{p}-\vec{A}(t))a^*(t) \times\exp[-iS(\vec{p},t,t')] \times\vec{\mathcal{E}}(t')\cdot\vec{d}(\vec{p}-\vec{A}(t'))a(t')+\text{c.c.}, \quad (1)$$

where $\vec{d}(\vec{p}-\vec{A}(t))$ is the field-free dipole transition matrix element between the ground state and the continuum state characterized by the velocity $\vec{v}=\vec{p}-\vec{A}(t)$, $\vec{p}$ denoting the canonical momentum, and $\vec{A}(t)$, the vector potential. $a(t)$ is the ground-state amplitude. Finally, $S(\vec{p},t,t')$ is the *quasiclassical action*, describing the motion of an electron moving in the laser field with a constant momentum $\vec{p}$,

$$S(\vec{p},t,t')=\int_{t'}^{t} dt''\left(\frac{(\vec{p}-\vec{A}(t''))^2}{2}+I_p\right). \quad (2)$$

The integral over momenta is estimated by means of the saddle-point method. The time dependent dipole moment becomes

$$\vec{x}(t)=i\int_0^\infty d\tau\left(\frac{\pi}{\nu+i\tau/2}\right)^{3/2}\vec{d}^{\,*}(\vec{p}_s-\vec{A}(t)) \times\exp[-iS(\vec{p}_s,t,\tau)] \times\vec{\mathcal{E}}(t')\cdot\vec{d}(\vec{p}_s-\vec{A}(t-\tau))|a(t)|^2+\text{c.c.}, \quad (3)$$

where $p_s(t)$ is the momentum for which the classical action S is stationary, and ν is a positive regularization constant. The time τ in Eq. (3) corresponds in classical terms to the time after which the electron returns to the nucleus. The so-called ''return times'' which contribute the most are shorter than one laser period. Contribution of longer times for multiple returns becomes negligible because of quantum diffusion of the wave packet. Actually, we have checked that, for high-order harmonics radiated from high-energy trajectories, quantum diffusion plays the same role as electron rescattering in the sense that they both discard the multiple returns. However, we have noticed that in the case of low-order harmonics (radiated from ''low energy'' trajectories; e.g, 17th and 23rd harmonics in neon), rescattering can have a stronger effect than quantum diffusion alone. Therefore, the dipole moment in Eq. (3) has been computed with either an unrestricted integration over τ (in xenon), or an integration restricted to $\tau\leqslant 2\pi/\omega$ (in argon and neon).

In the case of hydrogenlike atoms and transitions from s states, the field-free dipole matrix elements can be approximated by [13,14]

$$\vec{d}(\vec{p})=i\frac{2^{7/2}\alpha^{5/4}}{\pi}\frac{\vec{p}}{(\vec{p}^{\,2}+\alpha)^3}. \quad (4)$$

The Fourier series expansion of the time-dependent dipole provides the harmonic components of q order which are the source terms for harmonic generation.

The second step consists of solving numerically the equation describing the propagation of an electromagnetic wave through an isotropic, dielectric medium. The source term is the macroscopic polarization induced by the driving field. As mentioned above, its nonlinear components of q order are directly related to those of the atomic dipole. The calculation is done in the paraxial and slowly varying envelope approximations [10]. Furthermore, in the present work, depletion of the ground state, defocusing, and blueshifting of the fundamental are taken into account. Their influence on the har-

monic polarization state remain, however, marginal at the considered laser intensity ($I \leqslant 6\times10^{14}$ W/cm^2 for a neon atom).

B. Polarization of the harmonics

Any arbitrary elliptical field ($E_x e^{-i\phi_x}$, $E_y e^{-i\phi_y}$, 0) can be characterized by three parameters, e.g., E_x, E_y, and the phase difference $\delta = \phi_x - \phi_y$; the signed measures of the minor and the major axes and the polar angle ϕ of the latter, referred to as the orientation of the polarization; or the intensity, the ellipticity ϵ, and the orientation. It is straightforward to calculate the polarization properties of the harmonic field radiated by a single atom. Introducing the angles γ, such that $\tan(\gamma) = E_x/E_y$, and χ, such that $\epsilon = \tan(\chi)$, the ellipticity and orientation can be obtained from the simple expressions [15]

$$\sin(2\chi) = \sin(2\gamma)\sin(\delta),$$

$$\tan(2\phi) = \tan(2\gamma)\cos(\delta). \tag{5}$$

In the macroscopic case, however, the polarization varies in space over the spatial profile and in time over the time profile, through the intensity dependence of the qth component of the time-dependent dipole. As a result, the space- and time-averaged harmonic field, which can be measured in an experiment, is only partially polarized. The characterization of a partially polarized field is more demanding than for a completely polarized field, requiring knowledge of four parameters. This problem is described in several textbooks, for example, in Born and Wolf [15]. We here recall only the relevant ideas needed for our analysis. A partially polarized field can be described by a 2×2 coherence matrix or, equivalently, by the four Stokes parameters s_0, s_1, s_2, and s_3. The Stokes parameters are formally defined as averaged functions of the complex field components. Their interest resides in their physical interpretation. They can also be viewed as the results of simple experiments where the intensity of the light passing through the combination of a polarizer and a compensator is measured [15]. The Stokes parameters are defined by the four following relations (note that the convention in the numbering can be different in other textbooks, e.g., in [16]):

$$s_0 = \langle E_x{}^2 + E_y{}^2\rangle = I(0,0) + I(\pi/2,0),$$

$$s_1 = \langle E_x{}^2 - E_y{}^2\rangle = I(0,0) - I(\pi/2,0),$$

$$s_2 = 2\langle E_x E_y \cos(\delta)\rangle = I(\pi/4,0) - I(3\pi/4,0),$$

$$s_3 = 2\langle E_x E_y \sin(\delta)\rangle = I(\pi/4,\pi/2) - I(3\pi/4,\pi/2), \tag{6}$$

where the function $I(\theta,\eta)$ is the intensity of the light measured behind a polarizer making an angle θ with respect to the x axis when a retardation η is introduced between the x and the y components of the field. Thus, $I(\theta,\eta)$ reads as

$$I(\theta,\eta) = \int\int |E_x(r,t)\cos(\theta) + E_y(r,t)\sin(\theta)e^{i\eta}|^2 2\pi r\, dr\, dt. \tag{7}$$

We denote by a single symbol $\vec{s}$ the four parameters s_0, s_1, s_2, s_3. According to the above definition, s_0 is the time- and space-averaged intensity, so that normalized parameters s_i/s_0 are sometimes used [16]. Any partially polarized light, or more precisely the associated $\vec{s}$ vector can be written as the sum of a completely unpolarized wave, characterized by a vector $\vec{s}^{np}$, and a completely polarized wave, $\vec{s}^{p}$, which are independent of each other. This decomposition is unique [15]:

$$\vec{s} = \vec{s}^{p} + \vec{s}^{np}, \tag{8}$$

with

$$\vec{s}^{np} = (s_0 - \sqrt{s_1^2+s_2^2+s_3^2}, 0, 0, 0), \tag{9}$$

$$\vec{s}^{p} = (\sqrt{s_1^2+s_2^2+s_3^2}, s_1, s_2, s_3). \tag{10}$$

The degree of polarization $\mathcal{P}$ is defined as

$$\mathcal{P} = \sqrt{\frac{s_1^2+s_2^2+s_3^2}{s_0}} = \frac{s_0 - s_0^{np}}{s_0}, \tag{11}$$

where $s_0^{np} = s_0 - \sqrt{s_1^2+s_2^2+s_3^2}$. $\mathcal{P}$ is always lower or equal to 1. It is equal to 1 only for completely polarized radiation. The unpolarized part is a fully isotropic, uncoherent, ''natural'' light of averaged intensity s_0^{np}. The polarized part has the same Stokes parameters as the total field except for the intensity s_0^p which satisfies the characteristic relation

$$(s_0^p)^2 = s_1^2 + s_2^2 + s_3^2. \tag{12}$$

As shown in the Appendix, Eq. (12) is highly binding for the field it defines: it implies that this field has a given ellipticity ϵ and orientation ϕ, independent of time and space, so that only one parameter, the intensity, varies. The polarization of the polarized part of the harmonic radiation is characterized everywhere in space (after the nonlinear medium), at any time, by a constant ϵ [$=\tan(\chi)$] and a constant ϕ, given by the relations

$$\sin(2\chi) = \frac{s_3}{\sqrt{s_1^2+s_2^2+s_3^2}} = \mathrm{sgn}(s_3)\frac{\sqrt{(s_0 - s_0^{np})^2 - s_1^2 - s_2^2}}{(s_0 - s_0^{np})}, \tag{13}$$

$$\tan(2\phi) = \frac{s_2}{s_1}, \tag{14}$$

where $\mathrm{sgn}(s_3) = s_3/|s_3|$ is the sign of s_3. By definition, the orientation and ellipticity of the total partially polarized field are the orientation and ellipticity of the polarized part of the radiation. It is of interest to relate this mathematical definition to the (more physical) averages of the orientation and ellipticity of the total field. Let us introduce the intensity-weighted, averaged orientation and ellipticity of the total field defined by

$$\langle \tan(2\phi_t)\rangle = \frac{1}{s_0}\langle \tan(2\gamma)\cos(\delta)(E_x^2 + E_y^2)\rangle, \tag{15}$$

$$\langle \sin(2\chi_t)\rangle = \frac{1}{s_0}\langle \sin(2\gamma)\sin(\delta)(E_x^2+E_y^2)\rangle, \qquad (16)$$

where ϕ_t and χ_t are local variables relative to the total field. The averaged values reflect the polarization in the high-intensity regions of space or time: it gives a physical, hand-waving, interpretation to the ''macroscopic'' polarization of the harmonic field. For the orientation, we checked numerically, that in our experimental conditions where $\mathcal{P}\geqslant 0.7$, the orientation $\tan(2\phi)$ [Eq. (14)] was very close to the averaged value $\langle \tan(2\phi_t)\rangle$. The averaged elliptcity can be written as

$$\langle \sin(2\chi_t)\rangle = \frac{s_3}{s_0} = \mathcal{P}\sin(2\chi), \qquad (17)$$

which differs by the factor $\mathcal{P}$ from the definition of $\epsilon=\tan(\chi)$ [see Eq. (13)]. ϵ cannot be directly interpreted as a ''macroscopic'' ellipticity. However, the parameters in Eqs. (13,14) obviously coincide with either the weighted or the standard mean values of $\tan(2\phi)$ and $\sin(2\chi)$ when the intensity s_0^{np} becomes negligible, i.e., for a degree of polarization $\mathcal{P}$ close to 1. At least in this limit, the parameters defined in Eqs. (13,14) can be interpreted as averaged values characterizing an ''average'' polarization of the harmonic field.

Finally, the ellipticity can be expressed as

$$\epsilon=\tan(\chi)=\mathrm{sgn}(s_3)\sqrt{\frac{s_0-s_0^{np}-\sqrt{s_1^2+s_2^2}}{s_0-s_0^{np}+\sqrt{s_1^2+s_2^2}}}. \qquad (18)$$

This will be used for comparison with experimental data. It is important to note that the determination of the ellipticity requires the knowledge of either s_3 or s_0^{np}, in addition to the s_0, s_1, and s_2 parameters. In other words, the circularly polarized part of the radiation has to be determined in order to characterize completely the harmonic polarization state.

III. EXPERIMENTAL PROCEDURE

In our experiment, we did not determine s_3 or s_0^{np}, which means that we could not give a complete determination of the harmonic ellipticity. We now discuss in more detail how the other Stokes parameters were determined, before describing the experimental setup.

A. Experimental determination of the Stokes parameters

We follow the classical scheme adapted from [15] except that, for practical reasons, we rotate the electric-field vector $\langle \vec{E}_q\rangle$ in front of a fixed polarizer (simply by rotating the polarization of the fundamental field), instead of rotating a polarizer in front of a field with a fixed polarization. In our analysis, (x,y) represent the axes of our polarizer, while (x',y') is the reference frame bound to the fundamental polarization (x' parallel to the major axis). The angle between the x and x' axes is called ϕ_f (see Fig. 1). We note $\mathcal{E}'_x=E'_x e^{-i\phi'_x}$ and $\mathcal{E}'_y=E'_y e^{-i\phi'_y}$ the complex components of the harmonic light vector in the (x',y') frame, and we set

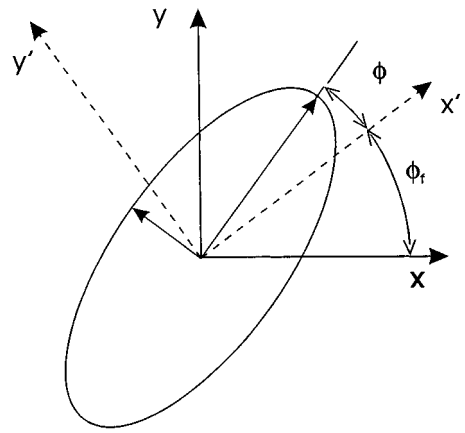

FIG. 1. Reference frame for the measurement of the harmonic polarization state. The (x',y') frame is bound to the major axis of the fundamental polarization. The angle ϕ is the offset angle between the major axes of the fundamental and harmonic ellipses.

$\delta'=\phi'_x-\phi'_y$. The polarizer is a reflecting element of reflectivity R_p along the x axis, and R_s along the y axis. Its action is only partial since neither R_p nor R_s is equal to zero. For the sake of completeness, let us assume that, by using the equivalent of a retardation plate, we could introduce a phaseshift η between the two components $\mathcal{E}'_y$ and $\mathcal{E}'_x$. The reflected intensity I_q measured after the polarizer is equal to

$$I_q(\epsilon_f,\phi_f,\eta)=R_p\langle \mathcal{E}_x\mathcal{E}_x^*\rangle+R_s\langle \mathcal{E}_y\mathcal{E}_y^*\rangle, \qquad (19)$$

where ϵ_f is the ellipticity of the fundamental. In terms of the field components in the (x',y') frame, I_q takes the form

$$I_q(\epsilon_f,\phi_f,\eta)=\frac{(R_s+R_p)}{2}s_0-\frac{(R_s-R_p)}{2}s_1\cos(2\phi_f)+\frac{(R_s-R_p)}{2}\langle 2E'_xE'_y\cos(\delta'-\eta)\rangle\sin(2\phi_f), \qquad (20)$$

where s_0 and s_1 are defined according to Eq. (6) in the (x',y') frame. When $\eta=0$, the second line of Eq. (20) is proportional to s_2, whereas, when $\eta=\pi/2$, it is proportional to s_3. Since, unfortunately, any phase shifting of one component of the XUV light relative to the perpendicular component is hardly feasible, only the s_1 and s_2 parameters were accessible in our experiment. We set $\eta=0$ in the following. Equation (20) can be written as

$$I_q(\epsilon_f,\phi_f,0)=\frac{R_s+R_p}{2}s_0-\frac{R_s-R_p}{2}\sqrt{s_1^2+s_2^2}\cos2(\phi_f+\phi), \qquad (21)$$

where we have introduced the angle ϕ defined by $\tan(2\phi)=s_2/s_1$. The transmitted intensity oscillates with the angle ϕ_f. The position of the maxima or minima can be used to determine the orientation of the harmonic field, while the amplitude of the modulations gives information on its degree of ellipticity. According to Eq. (14), ϕ can be directly interpreted as the polar angle of the major axis of $\langle \vec{E}_q\rangle$ in the

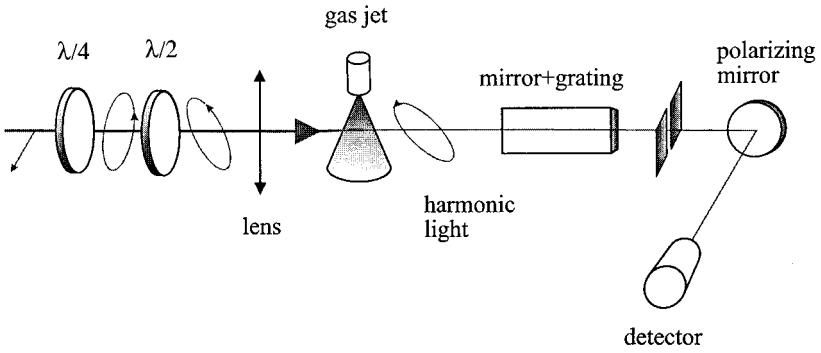

FIG. 2. Experimental setup for the measurements of the rotation angle and ellipticity of the harmonics. The polarization of the harmonic radiation is rotated in front of a fixed polarizing mirror.

(x',y') frame, or, in other words, the angle between the major axes of the fundamental and the harmonic polarization (see Fig. 1), i.e., the offset angle. $\phi_f+\phi$ is the polar angle for the major axis of $\langle \vec{E}_q \rangle$ in the (x,y) frame. From Eq. (21), we easily see that the maximum is obtained when $\phi_f+\phi=\pi/2$, i.e., when the major axis of the harmonic polarization is vertical, in the direction of the maximum reflectivity of the polarizer. The amplitude of the modulation of the transmitted intensity I_q does not provide a complete ellipticity determination unless the light is completely polarized. Let us introduce the parameter ϵ_{max}:

$$\epsilon_{max}=\sqrt{\frac{R_s I_{min}-R_p I_{max}}{R_s I_{max}-R_p I_{min}}}, \tag{22}$$

where

$$I_{max/min}=\frac{R_s+R_p}{2}s_0 \pm \frac{R_s-R_p}{2}\sqrt{s_1^2+s_2^2}. \tag{23}$$

I_{max} (I_{min}) are, respectively, the maximum and the minimum of the transmitted intensity I_q. The parameter ϵ_{max} can be expressed in terms of Stokes parameters as

$$\epsilon_{max}=\sqrt{\frac{s_0-\sqrt{s_1^2+s_2^2}}{s_0+\sqrt{s_1^2+s_2^2}}}. \tag{24}$$

The comparison with Eq. (18) clearly shows that ϵ_{max} is equal to the absolute value of the exact ellipiticity ϵ only if $s_0^{np}=0$ (i.e., for a completely polarized laser field). It can be interpreted as an *upper bound* of the ellipticity, since Eq. (18) is a slowly decreasing function of s_0^{np}. Note that the sign of the ellipticity (the sign of s_3) cannot be measured in our experiment.

B. Experimental setup

We now describe the experimental conditions in which harmonic generation was studied. The experimental setup is schematically displayed in Fig. 2. The experiment was performed in the femtosecond laser facility of the CEA-DRECAM in Saclay. The laser used is a titanium-sapphire system consisting of an oscillator, a regenerative amplifier, and a second amplifier (multipass), operating at a 20 Hz repetition rate. High-energy output of typically 50 mJ is achieved at 790 nm with a pulse duration of 150 fs. The beam has a 40 mm diameter before it is apertured and focused in a gas jet using a fused-silica lens of focal length $f=1$ m. The characteristics of the pulsed gas jet used in this experiment have been thoroughly described in [17]. The jet of gas is quite collimated, and the density profile is a quasi-Lorentzian distribution. In the present experiment, we estimate the peak pressure to about 10 mbar and the length of the medium (i.e., full width at half maximum of the density profile) to 1 mm. The laser beam focus was positioned at the center of the gas jet (with an uncertainty of 0.3 mm).

Adjusting the diaphragm before focusing is a convenient way to control the light intensity at focus in order to avoid significant ionization of the emitting medium. The peak intensity was estimated by measuring the number of harmonic photons as a function of the pulse energy; the curves obtained were then compared to the ones reported in [18], which were measured in very similar conditions and thoroughly calibrated. In the present work, the polarization measurements were performed at 10^{14} W/cm^2 in xenon, 2×10^{14} W/cm^2 in argon, and at 4 or 6×10^{14} W/cm^2 (depending on the harmonic order) in neon within a factor of 1.5 uncertainty. These intensities are significantly below the so-called saturation intensities for the three gases. Above saturation, ionization is significant so that depletion of the ground state and the effect of the free electrons (defocusing of the fundamental beam and additional phase mismatch) become important. These effects are nevertheless not negligible in our experimental conditions and are accounted for in the simulations. The confocal parameter b depends on the diaphragm aperture and therefore on the gas used to generate the harmonics. It varies between approximately 5 mm for neon to 20 mm for xenon. In the numerical simulations, we assumed the beam to be Gaussian.

After the interaction, the fundamental and harmonic lights were focused by a toroidal mirror of 1 m focal length and diffracted at grazing incidence on a plane grating (157° deviation, variable density of grooves around 700 grooves/mm). The exit slit of the spectrometer was set to 200 μm, corresponding to a 1 Å spectral resolution. This was sufficient to properly resolve two successive harmonics, but not to measure the spectral profile of each harmonic. (We checked that a 400 μm slit did not change the profiles.)

A silver-coated mirror at 45° incidence angle was installed between the output slit and the photomultiplier detector (see Fig. 1). It acts as a polarizer since its reflectivity is strongly polarization dependent ($R_s \ll R_p$). The incidence angle of 45° was chosen so that the R_s/R_p ratio or ''contrast'' is maximum. The higher the contrast (infinite for a perfect polarizer), the more accurate is the ellipticity measurement. In similar experiments carried out by Bucksbaum

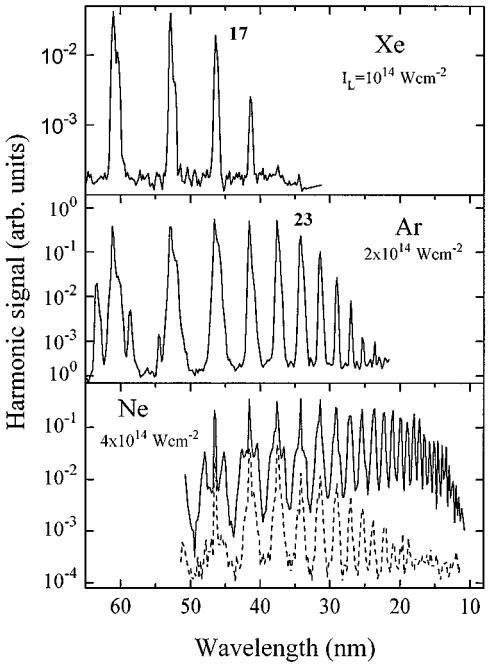

FIG. 3. Harmonic spectra measured with (a) the spectrometer only (——), in xenon, argon, and neon; (b) the spectrometer and the polarizing mirror in neon (- - -). The latter shows the decrease of the reflected intensity with energy, which limits reliable measurements to the 33rd order.

[9], the grating used for selecting the harmonics played the role of the polarizer, introducing a contrast R_s/R_p of about 2. The same contrast was measured with our spectrometer (mirror and grating at grazing incidence). With the addition of the mirror at 45 degrees incidence, however, a total contrast of 12 to 20 was achieved for radiation typically between 25 and 50 eV [19]. In the same range, the absolute reflectivities decrease from about 0.2 for s-polarized light (R_s) and 0.03 for p-polarized light (R_p) by at least one order of magnitude in each polarization. This is illustrated in the harmonic spectum measured in neon in Fig. 3. The intensity of the different harmonics, shown by the dashed line, regularly decreases as a function of harmonic order, while in the same conditions without the reflecting mirror, the plateau extends till the order 67 (solid line). The 29th harmonic in neon is the last for which ellipticity measurements could be performed with sufficient accuracy. Measurements of the orientation, not as demanding, were performed up to the 33rd harmonic.

The polarization of the fundamental beam was initially linear along the x horizontal axis. It was first made elliptical using a quarter-wave plate of zero-order. An angle α between a neutral axis of the plate and the x axis (see Fig. 2) introduces an ellipticity $\epsilon_f=\tan(\alpha)$. Changing the sign of α inverts the sense of rotation on the ellipse. The elliptical polarization was then rotated using a half-wave plate making an angle β with respect to the x axis. The angle ϕ_f is equal to $2\beta-\alpha$ and the measured intensity $I_q(\alpha,\beta)$ can easily be expressed as a function of the orientation $\phi_f(\beta,\alpha)$ of the fundamental field. A typical example corresponding to the 17th harmonic in neon is reported in Fig. 4 for linear ($\epsilon_f=0$) and elliptical [$\epsilon_f=\pm\tan(10°)$] polarization. The observed period of π agrees with the prediction of Eq. (21).

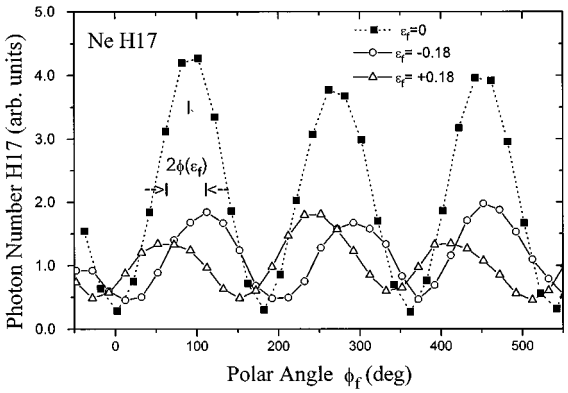

FIG. 4. Intensity of the 17th harmonic (I_{17}) measured after the polarizer, as a function of the polar angle ϕ_f of the major axis, for several ellipticities $\epsilon_f=0,\pm0.18$ of the fundamental polarization. The offset angle ϕ is directly obtained from the phase shift between the curves corresponding to ϵ_f and $-\epsilon_f$. The ellipticity upper bound ϵ_{max} is derived from the I_{max} and I_{min} measurements.

The parameters I_{max} and I_{min} leading to s_1, s_2 are derived from a fit of the form of Eq. (21). In the linear case, $\epsilon_f=0$, $\phi(\epsilon_f=0)=0$ and the I_{max}/I_{min} ratio gives the contrast R_s/R_p.

To determine the orientation angle, we use the symmetry relation $\phi(\epsilon_f)=-\phi(-\epsilon_f)$. It allows us to determine $\phi(\epsilon_f)$ as

$$\phi(\epsilon_f)=\frac{1}{2}[\phi_f(-\epsilon_f)-\phi_f(\epsilon_f)] \tag{25}$$

which is directly obtained by reading the difference between the angles corresponding to the maxima of $I_q(\epsilon_f,\phi_f)$ and $I_q(-\epsilon_f,\phi_f)$ in Fig. 4.

In the elliptical case, the measurements of I_{max} and I_{min} allow us to determine ϵ_{max}, upper limit to the absolute value of the true ellipticity ϵ [see Eq. (22)]. As for the rotation angle, we have the symmetry relation $\epsilon(-\epsilon_f)=-\epsilon(\epsilon_f)$ and $\epsilon_{max}(-\epsilon_f)=\epsilon_{max}(\epsilon_f)$. We measure independently $\epsilon_{max}(\epsilon_f)$ and $\epsilon_{max}(-\epsilon_f)$, and take the average value. These measurements do not provide the sign of the harmonic ellipticity: the parameter ϵ_{max} is defined as a positive quantity, which does not include the sign information. In the following (see Figs. 5–7), in order to plot and compare ϵ_{max} to the calculated ϵ in the full range of measurements, we attribute a sign to ϵ_{max}, which is the same as that of the calculated ϵ (and as that of the fundamental ϵ_f). In fact, we showed in [10] that, in conditions close to our experiment, the calculated ellipticity of the harmonic far field, after propagation and integration in time and space, kept the same sign as ϵ_f throughout the studied range. Note that it is not necessarily the case for the harmonic field generated locally, by a single atom (see, e.g., the single atom response for the 23rd harmonic in [10]).

In the experimental signal (Fig. 4), the positions of the maxima are more accurately determined from the fit than are the amplitude of the oscillations. Therefore, it is clear from Eqs. (21) and (22) that the uncertainty on the upper value ϵ_{max} of the ellipticity is larger than the one on the rotation angle [we have mentioned that in neon and for the highest harmonics 29, 33, the I_{min} signal was relatively low and

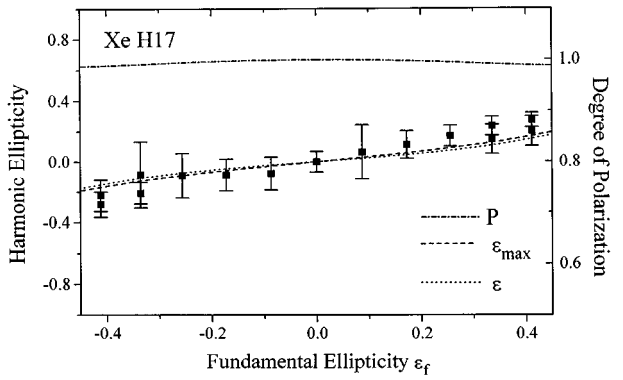

FIG. 5. Measured and calculated ellipticity upper bound ϵ_{max} (- - - -) for the 17th harmonic in xenon, as a function of ϵ_f; calculated ''true'' ellipticity ϵ $(\cdots)$; degree of polarization $\mathcal{P}$ $(\cdot-\cdot-\cdot)$. In Figs. 5–7, the sign of ϵ_{max} is chosen to be that of the calculated ϵ. The same confocal parameter b as for the offset angle is used in the calculations.

subsequently the uncertainty large: $\Delta I_{min}/I_{min}=1$ in the worse cases. An overestimate of I_{min} would lead to an overestimate of ϵ_{max} in Eq. (22)].

Let us mention a source of error in the I_q measurements, caused by the small but unavoidable birefringence of the entrance window to the vacuum chamber. This alters the ellipticity ϵ_f and orientation ϕ_f of the fundamental field, in a way which depends on the half-wave plate orientation. Even a very small birefringence, not observable in the visible range, prevents a reliable measurement of the intensity I_q, which is a very sensitive function of ϵ_f and ϕ_f. Several fused silica windows, of thickness 5 to 8 mm mounted with minimum constraints and accurately set perpendicular to the light propagation were tested. Although the birefringence of neither of them could be observed in the usual way, i.e., by detecting a variation of the transmitted light when rotating the window between crossed polarizers, it was clearly observable in the harmonic signal. The birefringence of the window leads to a modulation of I_q, which is only 2π periodic and not π periodic, as it should be, and to differences in the maxima obtained for ϵ_f and $-\epsilon_f$. The results presented in Fig. 4 and below were obtained with the ''best'' available window. The effect of the small birefringence induced by the window on the harmonic signal is still observ-

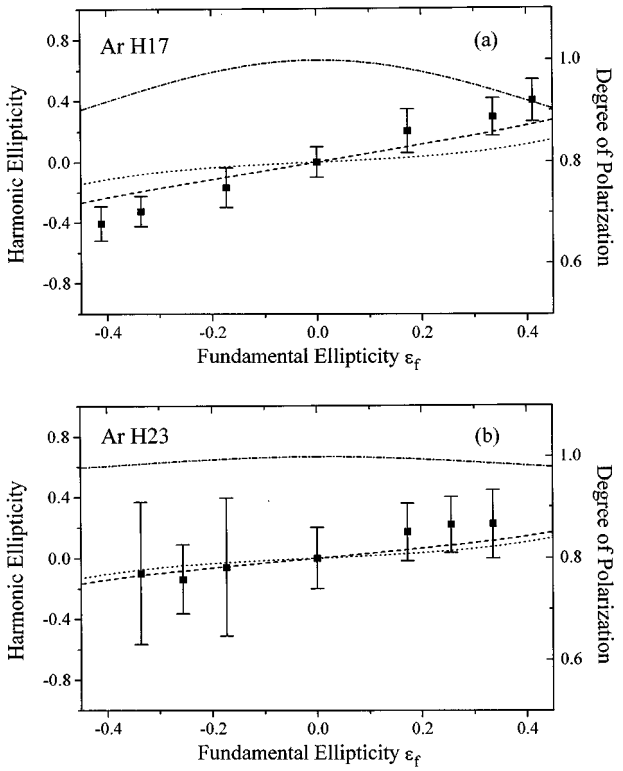

FIG. 6. Measured and calculated ellipticity upper bound ϵ_{max} (- - - -) for the (a) 23rd, (b) 17th harmonic in argon; calculated ''true'' ellipticity ϵ $(\cdots)$; degree of plarization $\mathcal{P}$ $(\cdot-\cdot-\cdot)$. Note that $|\epsilon_{max}-\epsilon|$ increases as $\mathcal{P}$ deviates from 1. The ''true'' ellipticity ϵ remains lower than ϵ_f.

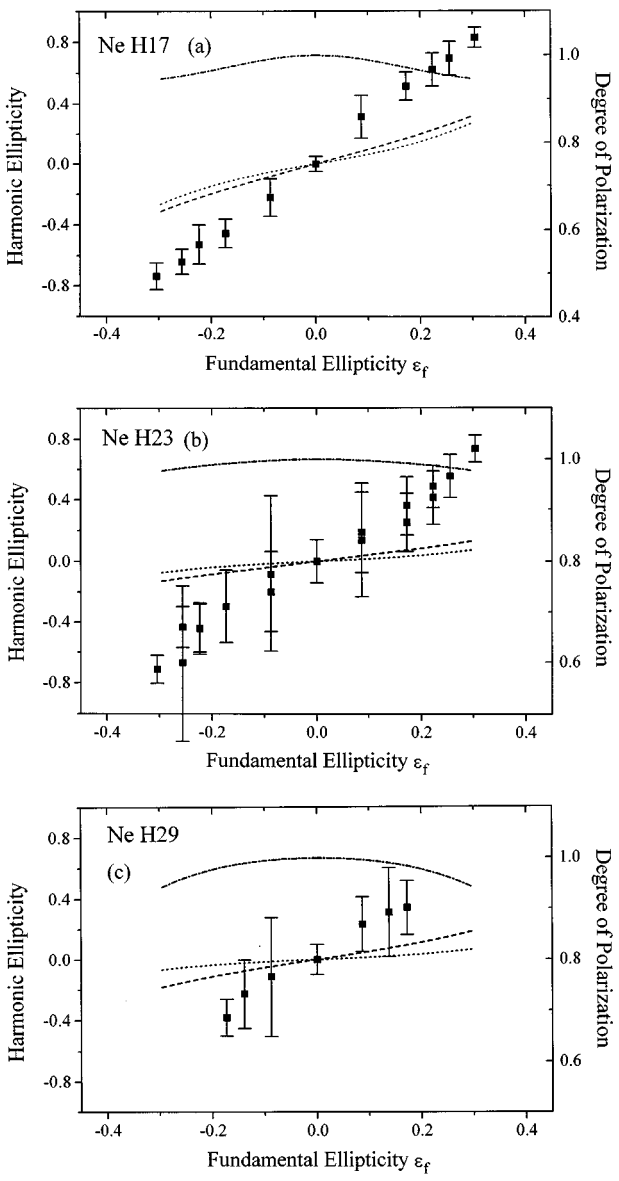

FIG. 7. Measured and calculated ellipticity upper bound ϵ_{max} (- - - -) for the (a) 17th, (b) 23rd, (c) 29th harmonic in neon; calculated ''true'' ellipticity ϵ $(\cdots)$; degree of plarization $\mathcal{P}$ $(\cdot-\cdot-\cdot)$. Note that both ϵ_{max} and ϵ increase as the harmonic moves far from the cutoff.

able as a 30% variation between the first two maxima in Fig. 4, corresponding to the two ellipticities ϵ_f and $-\epsilon_f$. This variation is, however, averaged in the fit.

The error bars shown in the figures for ellipticity presented below account for the two sources of error we have mentioned, i.e., the one on I_{min} and the one induced by birefringence effects.

IV. RESULTS

We performed systematic measurements in xenon, argon and neon, for the 17th, 23rd, 29th, and 33rd harmonics. (Note that, in our experimental conditions, the last two harmonics were observable only in neon, and the 23rd only in argon and neon.) In this way, we span, not only the gas and intensity, but also the position of the harmonic in the spectrum at the considered intensity. According to theoretical calculations [10], the variation of the rotation angle and the ellipticity with the laser ellipticity strongly depends on whether the harmonic is in the plateau or in the cutoff. The harmonic spectra obtained in the three rare gases at the considered laser intensities using linearly polarized light and no polarizing mirror are shown in Fig. 3. As an example, the 23rd harmonic is in the cutoff in argon, but in the plateau in neon. The 17th harmonic lies in the cutoff in xenon, while in the plateau in neon and argon, etc.

We present in parallel to the experimental results for the rotation angle and upper value of the ellipticity, the results of numerical simulations, using the method described in Sec. II. For argon and neon, the best comparison between measured and calculated values is obtained when taking account of the rescattering in an effective way, i.e., when restricting the integration over the return time τ to $\tau \leqslant 2\pi/\omega$ in the expression (3) of the dipole moment. The curves displayed in Figs. 8, 9, 6, and 7 are calculated with a restricted integration.

For xenon, the two calculations, either with or without the above restriction of the integration, give essentially the same results. The curves displayed in Figs. 10 and 5 are calculated with a full integration.

The simulations were found to be robust against variations as large as a factor of 2 of the intensity, the laser confocal parameter, and in general, the macroscopic parameters of the interaction. This makes the comparison between the experimental and theoretical results meaningful. It is worth stressing that the calculations are *ab initio*, without any parameter adjustment. We now describe in turn the results for the rotation angle and the ellipticity.

A. Rotation angle

In xenon, we restrict the analysis to the 17th harmonic, which is already in the cutoff at an intensity of 10^{14} W/cm^2. The result is shown in Fig. 10. The offset angle relative to the fundamental increases approximately linearly with the laser ellipticity, but remains very small, lower than 5° in the studied range. This is in good agreement with the theoretical prediction, shown by the dashed line. Note that, in Figs. 8–10, the experimental points and the calculated curve have been antisymmetrized with respect to $\epsilon_f = 0$, in order to match the range for the ellipticity measurements in the next section. The odd character of experimental offset angle ϕ is explicitly introduced in Eq. (25). In Figs. 8–10, the error bars are the ones computed from the standard deviations in the fit to the experimental data.

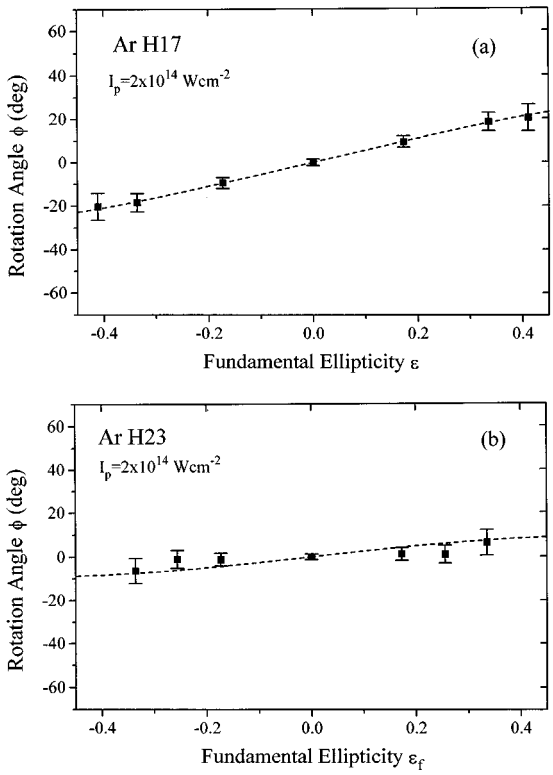

FIG. 8. Measured and calculated offset angle for the (a) 17th and (b) 23rd harmonic in argon, $b = 1$ cm.

In the case of argon, at an intensity of 2×10^{14} W/cm^2, the 17th and 23rd harmonics are, respectively, at the end of the plateau and in the cutoff. The offset angle for the 17th harmonic is significantly greater than the one for the 23rd (Fig. 8). This effect is well reproduced by the calculations.

In neon, the laser intensity is increased up to respectively 4×10^{14} W/cm^2 for the 17th and 23rd orders and 6×10^{14} W/cm^2 for the 29th and 33rd orders without excessive ionization of the emitting medium. All of these harmonics are well in the plateau region. In all our measurements, the rotation angle varies approximately linearly with the laser ellipticity. The results presented in Fig. 9 show a regular decrease of the offset angle as a function of the harmonic order. The comparison between the rotation angles obtained for the same harmonic order (the 17th and the 23rd) in the different rare gases leads to the conclusion that for a given laser ellipticity, the rotation angle strongly decreases from neon to xenon, i.e., as one becomes closer to the cutoff. In conclusion, the present set of data shows that it is the relative position of a given harmonic, either close to or far from the cutoff, which determines the slope of the offset angle as a function of the laser ellipticity, rather than the harmonic order itself or the emitting medium.

B. Harmonic ellipticity

As explained in Sec. III, due to the partial polarization of the harmonic light, the measurement of the contrast I_{max}/I_{min} leads to an upper bound ϵ_{max} [Eq. (24)] rather than to the harmonic ellipticity ϵ itself [Eq. (18)]. A misleading

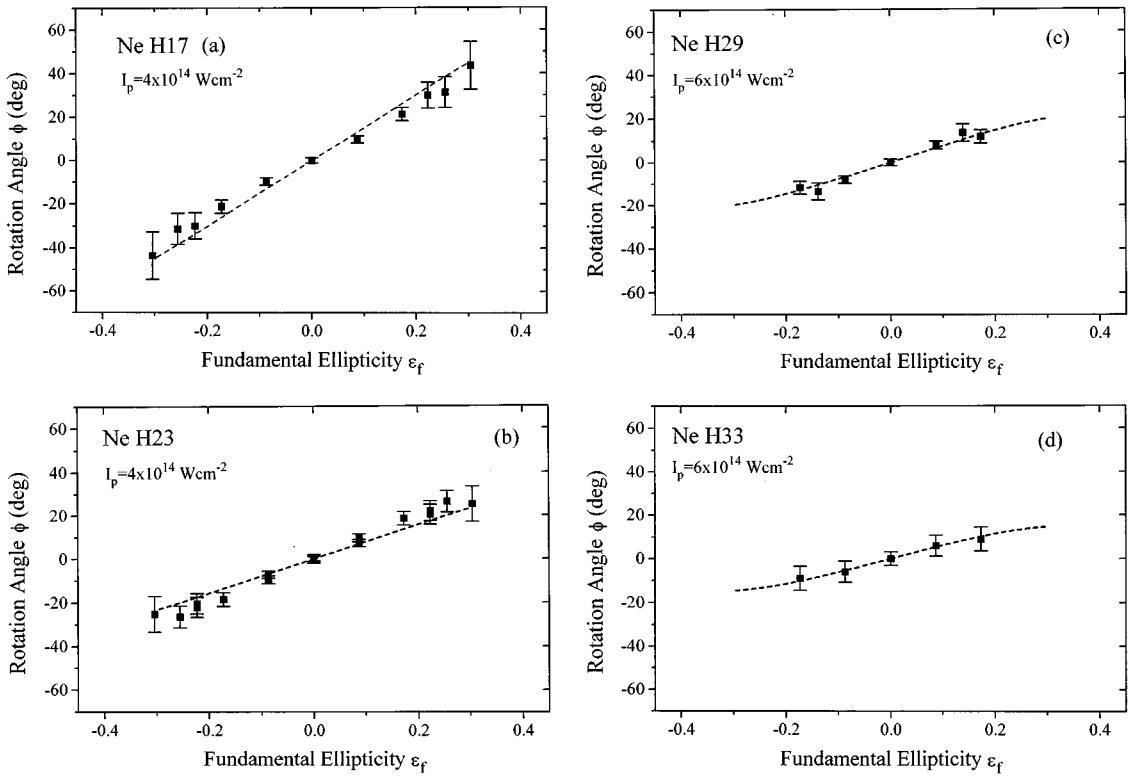

FIG. 9. Measured and calculated offset angle for the (a) 17th; (b) 23rd in neon, $b=0.5$ cm; (c) 29th; and (d) 33rd harmonic in neon, $b=0.5$ cm.

interpretation of the measured quantity, erroneously regarded as the ellipticity, may result in overestimating ϵ by up to a factor of 2 in our experimental conditions. In Figs. 5–7, we plot in the same graph, the signed ϵ_{max} from the experiment, and the calculated ϵ and signed ϵ_{max} (dotted and dashed lines, respectively) as functions of the laser intensity. We recall that the sign of signed ϵ_{max} is chosen as the one of calculated ϵ, so that both quantities appear to be odd functions of ϵ_f. In Figs. 5–7, for the sake of simplicity, the same label ϵ_{max} is used for signed ϵ_{max}. We also show, on a different scale indicated at the right in the figure, the calculated degree of polarization. In these measurements, we did not include the 33rd harmonic in neon, which was too weak to allow us to determine unambiguously I_{min}. As mentioned above, the error bars are computed from both the experimental uncertainty on I_{min} and the standard deviation in the fit from the data points.

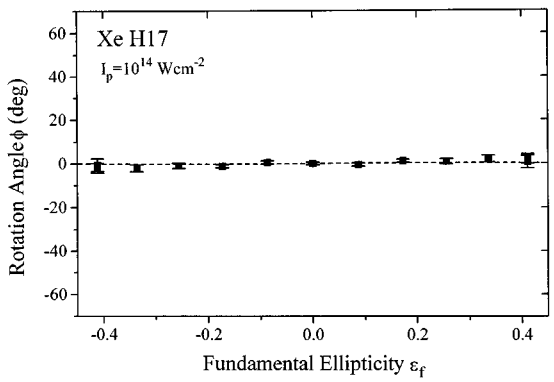

FIG. 10. Measured and calculated offset angle for the 17th harmonic in xenon, as a function of the fundamental ellipticity ϵ_f (here and in Fig. 5, full integration over τ in the dipole moment). Both experimental points and theoretical curve are symmetrized with respect to $\epsilon_f=0$. We use a confocal parameter $b=2$ cm in the calculation.

In xenon, the ellipticity upper bound for the 17th harmonic remains very small (Fig. 5). The same observation is made for the 23rd harmonic in argon [Fig. 6(a)]. These two harmonics are in the cutoff. An harmonic in the plateau but close to the cutoff (17th in argon) presents an ellipticity upper bound which is larger than the first two, but nevertheless smaller than the ellipticity of the driving field [Fig. 6(b)]. In each figure, we note that the smaller the degree $\mathcal{P}$ of polarization, the larger the difference between ϵ and ϵ_{max}.

Turning to neon, we observe an upper bound that is very large, even within the error bars. It is of the same order or even larger than the fundamental ellipticity. The calculated ϵ_{max} is in general lower than the experimental value. We tentatively attribute this discrepancy to the effect of rescattering, especially important for the low harmonics radiated from ''low energy'' trajectories. For the 17th (H17) and 23rd (H23), harmonic the contributing trajectories correspond to a kinetic energy of the electron of, respectively, 4.8 eV and 14.1 eV above the ionization threshold. At such a low energy in the atomic continuum, long-range Coulomb interaction may drastically affect the electron trajectory, and therefore the polarization of the harmonic light. Actually, the effective account for Coulomb scattering, as included in the model, may be not accurate enough. Note that for H17 in argon, energy of 10.6 eV is associated with the contributing trajec-

tories, and that the experimental value is already slightly larger than the computed one.

As in the rotation angle measurements, a general trend can be infered from the results. The variation of the ellipticity upper bound with the laser ellipticity is rather small for the harmonic in the cutoff, but increases significantly as the harmonic moves away from the cutoff.

A large ellipticity upper bound corresponds, in general, to a degree of polarization significantly smaller than 1, i.e., such that ϵ is substantially different from ϵ_{max}. In these conditions, any conclusion on the harmonic ellipticity based from contrast measurements is obviously hazardous. This should be the case for H17 in argon and H29 in neon (see the curves in Figs. 6 and 7), where the upper value ϵ_{max} and ellipticity ϵ differ at maximum by a factor of 2. However, in the case of xenon but also of argon, the good agreement obtained between the experimental results and the simulations for ϵ_{max} gives us enough confidence to conclude on the harmonic ellipticity, using the results of the numerical simulations shown in the dotted line. The ellipticity of the harmonic field appears to be always smaller than that of the driving field. It is about half of the laser degree of ellipticity when the harmonic is well in the plateau region. It is close to zero, i.e., the radiation is almost linearly polarized, when the harmonic is in the cutoff region of the spectrum. Although the comparison is much less convincing in neon, we tentatively assume that the conclusion stands for the different gases.

It has been demonstrated that the coherence properties of the harmonic light were optimized when the fundamental beam was focused far before the gas jet [20]. In that case, the considered harmonic is close to the cutoff region. On the basis of the present results, we can expect the harmonic radiation to be almost linearly polarized even if the driving field polarization is elliptically polarized.

V. CONCLUSION

We have presented measurements of the polarization state of high-order harmonics in xenon, argon, and neon. Large deviations from the polarization of the driving field were observed for the three gases and all considered harmonic orders. It seems that it is not the nature of the gas but rather the harmonic position in the spectrum that determines the harmonic polarization state. In the cutoff region, the harmonic ellipticity is much smaller than the fundamental ellipticity. A very small rotation angle of the harmonic polarization ellipse with respect to the fundamental one is observed. However, when the harmonic is far from the cutoff, its polarization has a significant degree of ellipticity, which nevertheless remains smaller than the fundamental ellipticity. Furthermore, the major axis of the harmonic polarization rotates by a large offset angle from the driving field polarization. This general trend is valid for all the harmonic orders and the three gases studied in this work.

The harmonic offset angle is very well reproduced in our theoretical model for the three gases. The computed upper bound of the harmonic ellipticity compares well with experiment for xenon and argon. It is found smaller for neon. For this gas with a high ionization potential, we assume that an exact account of Coulomb scattering should be necessary for improving the results on ellipticity. It is worth stressing that polarization measurements are a severe test for theoretical predictions. Except for the ellipticity in neon, the good agreement between theory and experiment indicates that our model describes well the dynamics of high-order harmonic generation and provides a good understanding of the mechanism.

ACKNOWLEDGMENTS

The authors are greatly indebted to Pascal Salières for fruitful discussions. They acknowledge the essential assistance of Pascal d'Oliveira, Pierre Meynadier, and Michel Perdrix, of the Femtoseconde Laser Facility of the CEA-DRECAM in Saclay. One of us (P.A.) acknowledges financial support from the Human Capital and Mobility program of the European Commission (Contract No. ERB4050PL921025). One of us (A.L.H.) acknowledges the support of the Swedish Natural Science Research Council.

APPENDIX

A completely polarized field is characterized by the relation [15]

$$s_0^2 = s_1^2 + s_2^2 + s_3^2, \tag{A1}$$

where the Stokes parameters are formally defined as averaged quantities in Eqs. (6). In this appendix, we show that Eq. (A1) is highly binding for the field in the sense that the ratio E_y/E_x and the phase difference $\delta = \phi_x - \phi_y$ (hence the orientation and ellipticity) should be constant throughout the whole time and space region of the average. From Eq. (A1), we easily show that

$$|\langle E_x E_y e^{i\delta}\rangle|^2 = \langle E_x^2\rangle\langle E_y^2\rangle. \tag{A2}$$

This equality is a limit case of a general Schwarz inequality. Let us consider the following averaged expression:

$$\langle (E_x + \lambda E_y e^{i\delta})(E_x + \lambda^* E_y e^{-i\delta})\rangle \geqslant 0, \tag{A3}$$

which is always positive or zero for any complex number $\lambda = \mu + i\nu$. According to Eq. (A2), the inequality (A3) reduces to the simple form

$$\left(\mu + \frac{\langle E_x E_y \cos\delta\rangle}{\langle E_y^2\rangle}\right)^2 + \left(\nu - \frac{\langle E_x E_y \sin\delta\rangle}{\langle E_y^2\rangle}\right)^2 \geqslant 0. \tag{A4}$$

It is clear that there exists two values μ and ν, or $\lambda = -(s_2 - is_3)/(s_0 - s_1)$, for which the expression is zero. As a result, the quantity averaged in Eq. (A3), which is always positive or zero, should be zero everywhere for the given λ. We can write at each point in time and space:

$$\frac{E_y}{E_x} e^{i\delta} = -\lambda^{-1} = \frac{s_2 + is_3}{s_0 + s_1}. \tag{A5}$$

It follows that $\tan(\gamma) = E_y/E_x$ and δ are constant in the region of averaging. The same is true for the variables χ and

ϕ defining locally the ellipticity and the orientation, since they are functions of γ and δ given by Eqs. (5). It is easy to obtain from Eq. (A5) their expressions in terms of the Stokes parameters:

$$\sin(2\chi)=\sin(2\gamma)\sin(\delta)=\frac{s_3}{s_0}, \tag{A6}$$

$$\tan(2\phi)=\tan(2\gamma)\cos(\delta)=\frac{s_2}{s_1},$$

in agreement with Eqs. (14)–(13). The parameters $\tan(\chi)$ and ϕ, initially defined as local variables, get therefore the meaning of a macroscopic ellipticity and orientation of the polarized field.

[1] K. C. Kulander, K. J. Schafer, and J. L. Krause, in *Super-Intense Laser-Atom Physics*, Vol. 316 of *NATO Advanced Study Institute, Series B: Physics*, edited by B. Piraux, A. L'Huillier, and K. Rzążewski (Plenum Press, New York, 1993), p. 95.

[2] P. B. Corkum, Phys. Rev. Lett. **71**, 1994 (1993).

[3] K. S. Budil, P. Salières, A. L'Huillier, T. Ditmire, and M. D. Perry, Phys. Rev. A **48**, R3437 (1993).

[4] P. Dietrich, N. H. Burnett, M. Yu. Ivanov, and P. B. Corkum, Phys. Rev. A **50**, R3585 (1995).

[5] Y. Liang, M. V. Ammosov, and S. L. Chin, J. Phys. B **27**, 1296 (1994).

[6] N. H. Burnett, C. Kan, and P. B. Corkum, Phys. Rev. A **51**, R3418 (1995).

[7] I. Mercer, E. Mevel, R. Zerne, A. L'Huillier, Ph. Antoine, and C.-G. Wahlström Phys. Rev. Lett. **77**, 1731 (1996).

[8] P. B. Corkum, N. H. Burnett, and M. Y. Ivanov, Opt. Lett. **19**, 1870 (1994); M. Yu. Ivanov, P. B. Corkum, T. Zuo, and A. Bandrauk, Phys. Rev. Lett. **74**, 2933 (1995).

[9] F. A. Weihe, S. K. Dutta, G. Korn, D. Du, P. H. Bucksbaum, and P. L. Shkolnikov, Phys. Rev. A **51**, R3433 (1995).

[10] Ph. Antoine, A. L'Huillier, M. Lewenstein, P. Salières, and B. Carré, Phys. Rev. A **53**, 1725 (1996).

[11] A. Lohr, S. Long, W. Becker, and J. K. McIver, in *Super-Intense Laser-Atom Physics*, *NATO Advanced Study Institute Series B: Physics*, edited by M. Fedorov and H. G. Muller (Plenum Press, New York, 1996), p. 477.

[12] L. V. Keldysh, Zh. Eksp. Teor. Fiz. **47**, 1945 (1964) [Sov. Phys. JETP **20**, 1307 (1965)]; F. Faisal, J. Phys. B **6**, L312 (1973); H. R. Reiss, Phys. Rev. A **22**, 1786 (1980).

[13] M. Lewenstein, Ph. Balcou, M. Yu. Ivanov, A. L'Huillier, and P. Corkum, Phys. Rev. A **49**, 2117 (1994).

[14] H. A. Bethe and E. E. Salpeter, *Quantum Mechanics of One and Two Electron Atoms* (Academic, New York, 1957).

[15] M. Born and E. Wolf, *Principles of Optics* (Pergamon Press, New York, 1964).

[16] L. D. Landau and E. M. Lifchitz, *The Classical Theory of Fields* (Pergamon Press, Oxford, 1962).

[17] C. Altucci, T. Starczewski, B. Carré, A. L'Huillier, and C.-G. Wahlström, J. Opt. Soc. Am. B **13**, 148 (1996).

[18] C.-G. Wahlström, J. Larsson, A. Persson, T. Starczewski, S. Svanberg, P. Salières, Ph. Balcou, and A. L'Huillier, Phys. Rev. A **48**, 4709 (1993).

[19] E. Palik, *Handbook of Optical Constants of Solids* (Academic Press, Orlando, 1985).

[20] P. Salières, A. L'Huillier, and M. Lewenstein, Phys. Rev. Lett. **75**, 3376 (1995).